Contents lists available at ScienceDirect

Mechanical Systems and Signal Processing

journal homepage: www.elsevier.com/locate/ymssp

Highlights

High performance raster scanning of atomic force microscopy using Model-free Repetitive Control

Mechanical Systems and Signal Processing xxx (xxxx) xxx

Linlin Li, Andrew J. Fleming, Yuen K. Yong, Sumeet S. Aphale, LiMin Zhu*

- The Model-free Repetitive Control is proposed for rejecting periodic tracking errors.
- This method handles the problem of model uncertainties met in practical applications.
- The design and stability analysis of the proposed method are presented in detail.
- Experimental tracking and coupling compensation of an AFM scanner are validated.

Contents lists available at ScienceDirect

Mechanical Systems and Signal Processing

journal homepage: www.elsevier.com/locate/ymssp

High performance raster scanning of atomic force microscopy using Model-free Repetitive Control

Linlin Li [a,b], Andrew J. Fleming [c], Yuen K. Yong [c], Sumeet S. Aphale [d], LiMin Zhu [a,e,*]

[a] State Key Laboratory of Mechanical System and Vibration, School of Mechanical Engineering, Shanghai Jiao Tong University, Shanghai 200240, China
[b] State Key Laboratory of Fluid Power and Mechatronic Systems, Zhejiang University, Hangzhou 310027, China
[c] School of Electrical Engineering and Computing, University of Newcastle, Callaghan NSW 2308, Australia
[d] The Artificial intelligence, Robotics and Mechatronic Systems Group (ARMS), School of Engineering, University of Aberdeen, Aberdeen AB24 3UE, UK
[e] The Shanghai Key Laboratory of Networked Manufacturing and Enterprise Information, Shanghai 200240, China

ARTICLE INFO

Communicated by J. RODELLAR

Keywords:
Atomic force microscopy
Raster scanning
Tracking control
Repetitive control
Cross-coupling compensation

ABSTRACT

The image quality of an atomic force microscope highly depends on the tracking performance of the lateral X–Y axis scanner. To reduce the requirement for accurate system models, this article describes a method based on Model-free Repetitive Control (MFRC) for high performance control of fast triangular trajectories in the X-axis while simultaneously achieving coupling compensation from the X-axis to Y-axis. The design and stability analysis of the MFRC scheme are presented in detail. The tracking results are experimentally evaluated with a range of different load conditions, showing the efficacy of the method with large variations in plant dynamics. To address the coupling from the X-axis to the Y-axis while tracking the non-periodic staircase trajectories, a pre-learning step is used to generate the compensation signals, which are combined with the baseline Proportional–Integral (PI) control in a feedforward manner in real-time implementations. This approach is also applied to address the problem of longer convergence if needed. Experimental tracking control and coupling compensation is demonstrated on a commercially available piezo-actuated scanner. The proposed method reduces the root-mean-square coupled tracking errors in Y-axis from 191.4 nm in open-loop control or 194.6 nm with PI control, to 2.8 nm with PI+MFRC control at 100 Hz tracking frequency, which demonstrates the significant improvement achieved by the proposed method.

1. Introduction

Several discoveries in life science, information, materials, and other disciplines, rely on the extraordinary features of Atomic Force Microscopes (AFMs) for imaging, characterizing, and manipulating matter with a resolution down to the nanoscale [1–3]. In imaging applications, the AFM employs a cantilever with a sharp probe to interrogate over a sample using a piezo-actuated scanner. The surface height of the sample causes the cantilever to deflect due to the probe-sample interaction force. This interaction force is regulated using the Z-axis (vertical) controller to keep the deflection of the cantilever constant. The topography of the sample is measured by the movement or control voltage in the Z-axis for every imaging point, which is then used to produce the 3-D topographical representation of the sample along the scanning trajectories. From its basic principle, it is known that the accuracy

* Corresponding author at: State Key Laboratory of Mechanical System and Vibration, School of Mechanical Engineering, Shanghai Jiao Tong University, Shanghai 200240, China.
E-mail address: zhulm@sjtu.edu.cn (L. Zhu).

https://doi.org/10.1016/j.ymssp.2022.109027
Received 12 October 2021; Received in revised form 11 February 2022; Accepted 7 March 2022

of the captured AFM images highly relies on the tracking precision of the desired scanning trajectory. Commonly, raster scanning is selected to generate the AFM images, in which the fast axis (X-axis) is actuated with a triangular signal and the slow axis (Y-axis) is actuated with the corresponding staircase or ramp-case signals [4,5]. To maximize scanning rate for dynamic imaging, there are multiple challenges that degrade the tracking performance of raster scanning and thus image quality. These include the hysteresis nonlinearity possessed by the piezoelectric actuators, the lightly-damped resonance of the mechanism, and the cross-coupling effect between the scanning axes [6]. In particular, under high-frequency inputs, the nonlinearities would be coupled with the vibrations associated with the lightly-damped resonance, which complicates the control design and limits the speed at which high-precision AFM images can be obtained [7,8].

During the past decades, significant improvements to the above issues have been made [5,9–11]. To reduce the effect of hysteresis, several model-based modeling and compensation methods have been developed, such as the operator-based models [12,13] (e.g. Prandtl–Ishlinskii model and Preisach model), intelligent models [14] (e.g. neural-network model and support vector machine model). It should be noted that the modeling and inversion of the hysteresis is not trivial, and it may need to be repeated for multiple applications. When hysteresis is coupled with lightly-damped resonant modes, the compensation performance can degrade dramatically. A variety of control techniques have been developed to address the vibrational problems on the basis of advanced hardware design [15–17], which include feedforward approaches [18,19], such as input shaping, optimal trajectory design, and notch-filter-based techniques, and feedback approaches, such as positive position feedback and its extensions [20,21], integral resonant control [22], and delayed position feedback control [23]. Among those techniques, the closed-loop approaches have better robustness to plant variations in practical implementations, so they are more widely utilized than feedforward approaches [11,24,25]. Further, to realize the tracking application of the nanopositioners, the tracking controllers are usually incorporated with the above control techniques for mitigating the residual nonlinearities and other disturbances. For tracking periodic trajectories, the highest performing methods are the learning-based schemes, repetitive control [26–28] and iterative control [7,29]. Specifically, it is analyzed in [8] that, the tracking errors induced by the hysteresis nonlinearity exhibit periodic behaviors under periodic inputs, and thus can be mitigated by these learning-based schemes, making it rather simple for high-precision raster scanning of AFM. It should be noted that in these developments, the multiple-axis scanners are normally treated as single input and single output systems, where the cross-coupling is neglected. In fact, the cross-coupling effect would become prominent in large-range and high-speed scanning operations, especially for these popularly used commercial tube-type scanners, which would cause tilting and other artifacts in the AFM images [6].

The three main research efforts for cross-coupling compensation in the field are (i) model-based cross-coupling compensation control; (ii) feedback tracking control, and (iii) learning-based schemes. For model-based cross-coupling compensation control, the main idea is to construct the inverse cross-coupling model using different techniques (such as Prandtl–Ishlinskii model [30] and MIMO model predictive control method [31,32]). The inverse mode is then used to compensate the cross-coupling effect by the feedforward method. However, the cross-coupling usually include complex dynamics, which make the modeling procedure very challenging. For feedback tracking control, the idea of this method is to regard the cross-coupling effects as output disturbances and compensate them by tracking control techniques, such as H_∞ control [33] and linear quadratic Gaussian control [34]. For learning-based schemes, it is experimentally investigated in [6] that, under periodic inputs, the tracking errors induced by the coupling effect result in periodic behaviors, which allows a new way for cross-coupling compensation. During raster scanning, the main coupling effect is the influence of the fast axis on the slow axis, which leads to the triangularization of the staircase trajectory, and possibly large tracking errors. In this sense, the modified repetitive control is successfully implemented to compensate for the tracking errors that result from the coupling of the fast axis on the slow axis, and therefore high-precision raster scanning with a scanning rate of 40 Hz is achieved [6]. It should be noted that such modified repetitive control requires accurate modeling of the inverse system dynamics for best performance. There are several difficulties associated with plant inversion, including multiple modes [35], non-minimum phase zeros [8], and model uncertainties due to variations in loads masses, temperature, and humidity while operating the AFMs [36].

Focusing the above difficulties, this article describes an improved method of Model-free Repetitive Control (MFRC) for applications like AFM which require tracking control of a fast axis and cross-coupling compensation of a slower axis. In order to avoid modeling the inverse system dynamics, a non-causal FIR low-pass filter is introduced into the repetitive module which has the advantage of zero phase-lag. This replaces the normally used low-pass zero-phase filter and the inversion of system dynamics in traditional repetitive control. The stability and convergence analysis is presented in detail to provide criteria for parameters determination. To achieve better tracking performance with limited bandwidth of the FIR low-pass filter, smoothed raster scanning [37] is selected in this work, which preserves the same imaging trajectory but with lower high-frequency components compared to traditional raster scanning. With the objective of fast convergence for the fast axis and tracking of the non-periodic staircase trajectory for the slowaxis during AFM raster scanning, a pre-learning method is utilized to obtain the effective control signals for both lateral axes, which is then used as feedforward control. This approach combines a baseline tracking controller for handling non-periodic disturbances and trajectories. Finally, AFM imaging results are presented to visually demonstrate the advantages of the proposed method.

The distinguished contributions of this paper can be summarized as follows:

(1) Tailored for the raster scanning of AFMs, the Model-free Repetitive Control is developed for tracking periodic trajectories in the X-axis and rejecting the corresponding coupled tracking errors in the Y-axis. This addresses the universal problem of model uncertainties encountered in practical AFM applications especially due to load change on the scanner.

(2) To handle the excessive iterations before convergence and the aperiodicity of the staircase trajectories in the Y-axis, a pre-learning step is employed to generate the effective control signals, which works in parallel with the baseline tracking controller in a feedforward manner.

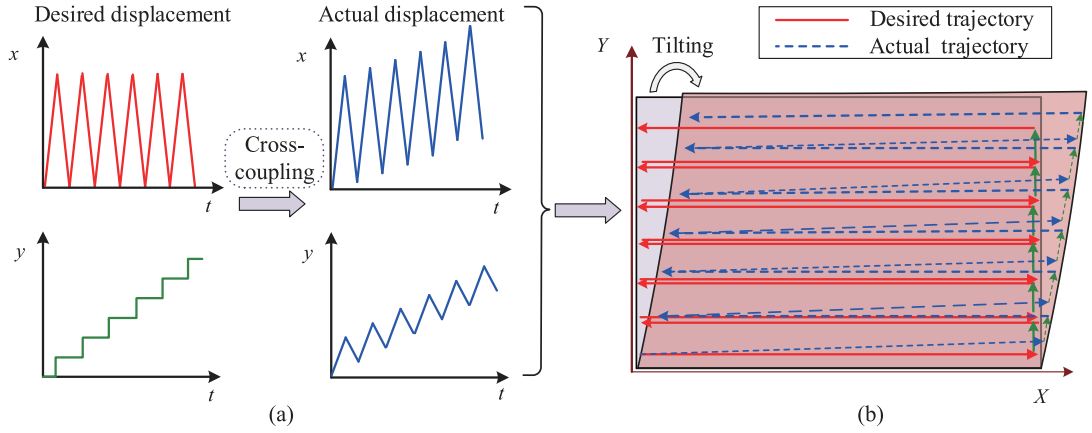

Fig. 1. Cross-coupling effect between the lateral X–Y axis in raster scanning of AFM.

(3) Experimental reference tracking and coupling compensation are demonstrated for AFM applications. The images are obtained using a commercially available piezo-actuated scanner, where high-precision raster scanning is demonstrated at 100 Hz, showing the advantages of the proposed schemes.

This paper is outlined as follows. Section 2 provides the basic information of the cross-coupling effect. Section 3 presents the design of the MFRC based scheme, and its stability analysis. Section 4 presents the details of the experimental setup and the controller performance. The experimental results, including the convergence analysis, tracking results and the AFM imaging results are demonstrated in Section 5 showing the advantages of the proposed scheme for high performance raster scanning. Section 6 summarizes this paper.

2. Cross-coupling information

The cross-coupling effect is significant in many multiple-axis motion control applications. Although several cutting edge mechanical designs can minimize this adverse effect, it cannot be completely avoided due to the errors in machining and assembly [15,17]. In AFM applications, cross-coupling distorts the scanning trajectories and may introduce artifacts into the captured image [4,6]. Specially, in raster scanning, the coupling from the fast scanning X-axis on the slow scanning Y-axis causes triangularization of the desired staircase trajectory. Similarly, cross-coupling from the Y-axis on the X-axis causes a drift of the desired triangular trajectory, as illustrated in Fig. 1. Generally speaking, as the high-frequency components and the amplitude of the triangular trajectory is much greater than that of the staircase trajectory [38], the Y-axis itself mainly suffers from the coupling effect. Therefore, this work focuses mainly on the dominant coupling effect from the X-axis on the Y-axis.

It is investigated in [6] that the tracking errors of the Y-axis induced by the coupling effect are found to exhibit periodic characteristics when the X-axis is following a triangular trajectory; therefore, the error can be regarded as a periodic output disturbance in the Y-axis. To guarantee the stability of the proposed scheme (which will be provided in detail in Section 3.2), the passband of the designed non-causal FIR low-pass filter is set to a limited range. Since the system bandwidth is limited, high-frequency components of the tracking error are not effectively suppressed. An alternative is to use a smoothed raster scanning method [37] which preserves the original imaging trajectory. To investigate the coupling effect, the spectra of the Y-axis position are analyzed and plotted in Fig. 2(a) and (b) respectively, when the X-axis is precisely tracking the smoothed triangular trajectory and the triangular trajectory with the frequency of 10 Hz. More information concerning the smoothed raster scanning method refers to [37]. It can be observed that tracking errors induced by the coupling effect have periodic characteristics in these two scanning cases, and thus can both be regarded as periodic disturbances injected to the output of Y-axis. Furthermore, as the high-frequency components of the smoothed trajectory are reduced (investigated in [37]), the high-frequency components of the coupled tracking errors decrease correspondingly. Therefore, the tracking performance can be improved using the smoothed raster scanning, which will be comparatively presented in detail in Section 5. Based on these observations, the Model-free Repetitive Control (MFRC) is developed in this work for control of both lateral axes in high performance raster scanning of AFMs.

3. Controller design

In the section, the Model-free Repetitive Control is designed for both lateral axes. The stability analysis is also provided as a criterion of parameter selection.

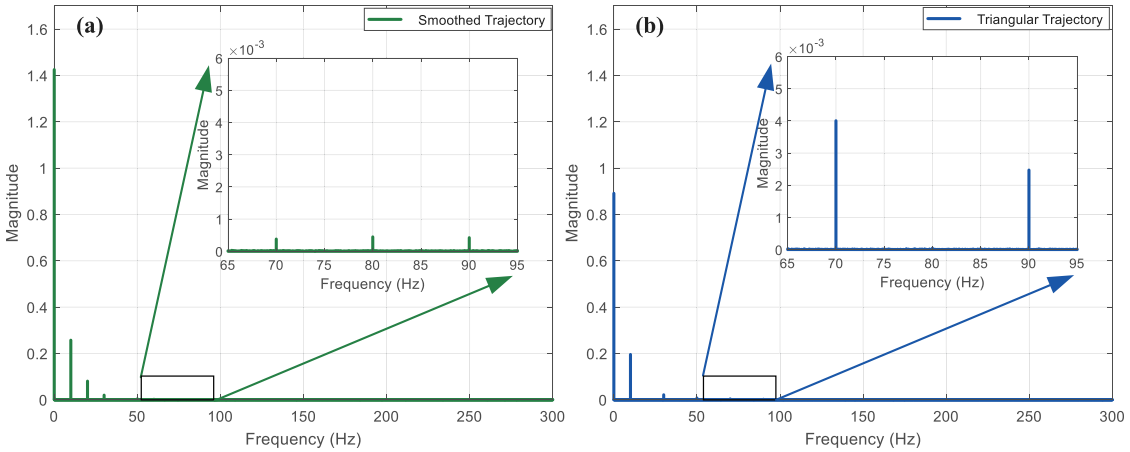

Fig. 2. Spectra of the displacement in the Y-axis when the X-axis is tracking different 10 Hz periodic trajectories: (a) Smoothed triangular trajectory; (b) Triangular trajectory.

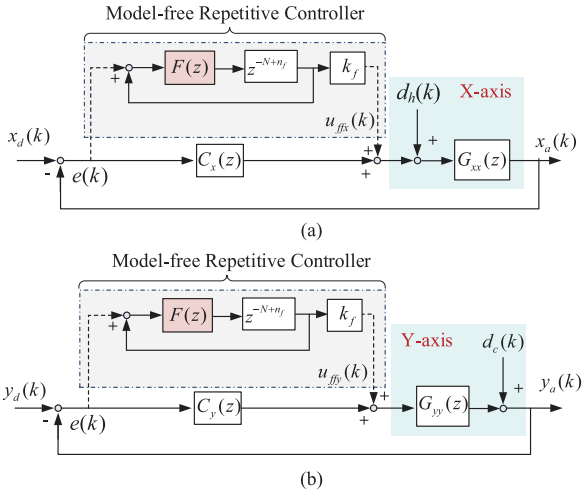

Fig. 3. Block diagrams of the MFRC based scheme: (a) X-axis; (b) Y-axis.

3.1. Design of the Model-free Repetitive Control based scheme

For periodic inputs, it is analyzed in [6,8] that (i) the hysteresis nonlinearity can be regarded as a bounded periodic input disturbances $d_h(k)$, and (ii) the coupling effect to the other axis can be seen as periodic output disturbances $d_c(k)$ as shown in Fig. 3. In this case, the repetitive control becomes an attractive method for achieving high-precision raster scanning. With the objective of handling the difficulties associated with plant inversion encountered in most repetitive control design, the Model-free Repetitive Control (MFRC) is developed for both lateral axes, which aims for tracking control of the X-axis and coupling compensation for the Y-axis in raster scanning.

Considering the raster scanning, the coupled lateral system can be simplified as Fig. 3, where $G_{xx}(z)$ and $G_{yy}(z)$ represents the linear dynamics of the X-axis and Y-axis, respectively. Due to the low variations of the staircase trajectory for Y-axis, the hysteresis nonlinearity of the Y-axis is not considered in Fig. 3. With the minor coupling errors from the Y-axis to the X-axis, this coupling error is not emphasized in this work. The items $x_d(k)$ and $x_a(k)$ are the desired trajectory and the actual trajectory for the X-axis, respectively. The items $y_d(k)$ and $y_a(k)$ are the desired trajectory and the actual trajectory for the Y-axis. As a plugged-in module, the developed MFRC is designed in parallel with the baseline tracking controller ($C_x(z)$ for X-axis and $C_y(z)$ for X-axis), whose block diagrams are shown in Fig. 3. In MFRC, a non-causal FIR low-pass filter

$$H(z) = \sum_{i=-n_f}^{n_f} h(i) z^{-i} \tag{1}$$

is introduced into the repetitive loop, instead of the general two-step design of the low-pass filter and inversion of the plant dynamics, where n_f is the parameter determining the filter length (order), and $h(i)$ is filter coefficients. In this way, the complicated modeling process of the inverse dynamics can be avoided, which significantly reduces the problem of model uncertainties and implementation complexity. As for the delayed part z^{-N} in Fig. 3, $N = f_s/f_d$ is the number of delayed points, where f_s and f_d denote the sampling rate and the desired scanning rate, respectively. The non-causality of $H(z)$ will be supplemented by the delayed part z^{-N} in real-time implementation, which becomes

$$F(z) = \sum_{i=0}^{2n_f} h(i) z^{-i} \tag{2}$$

The actual points of the delayed part is therefore reduced to $N - n_f$. k_f is the gain of the developed MFRC.

There are many choices for the baseline tracking controller, such as Proportional–Integral (PI) control [39] and sliding mode control [40]. With its simple structure, the PI control is selected in this work. It can be concluded from the above analysis that there are only two items ($F(z)$ and k_f) that are required to be determined in MFRC, making it rather simple for practical applications.

3.2. Stability analysis

To provide criteria for parameter determination, the condition of stability is analyzed as follows. As the control schemes for the X-axis and Y-axis are identical, the stability analysis for the X-axis (Fig. 3(a)) is presented as example. Before the design of the developed MFRC, the system with the baseline tracking controller should be designed to ensure asymptotical stability, which implies that $1 + C_x(z)G_{xx}(z) = 0$ has no roots outside of the unit circle in the z-plane. Assuming this condition is satisfied first, the sensitivity function is

$$\frac{e(k)}{x_a(k)} = \frac{1 - F(z)z^{-N+n_f}}{[1 + C_x(z)G_{xx}(z)][1 - F(z)z^{-N+n_f}] + F(z)z^{-N+n_f} k_f G_{xx}(z)} \tag{3}$$

Thus, the polynomial of the closed-loop characteristics is (the symbol of z-domain is omitted in the follow derivation for simplicity)

$$\begin{aligned} D(z) &= (1 + C_x G_{xx})(1 - F z^{-N+n_f}) + (F z^{-N+n_f} k_f G_{xx}) \\ &= (1 + C_x G_{xx})(1 - F z^{-N+n_f} + \tfrac{F z^{-N+n_f} k_f G_{xx}}{1 + C_x G_{xx}}) \end{aligned} \tag{4}$$

As the first item is asymptotically stable by the previous assumption, the stability depends on the second item only. According to the Small-gain Theorem, the system is asymptotically stable if

$$\left| -F z^{-N+n_f} + \frac{F z^{-N+n_f} k_f G_{xx}}{1 + C_x G_{xx}} \right|_{z=e^{j\omega T_s}} < 1, \omega \in [0, \pi/T_s] \tag{5}$$

in which T_s is the sampling time. It is obvious that $\left| z^{-N+n_f} \right|_{z=e^{j\omega T_s}} = 1$, then we have

$$\left| -F + \frac{F k_f G_{xx}}{1 + C_x G_{xx}} \right|_{z=e^{j\omega T_s}} < 1, \omega \in [0, \pi/T_s] \tag{6}$$

which can be expressed as

$$0 < \left| \frac{k_f G_{xx}}{1 + C_x G_{xx}} \right|_{z=e^{j\omega T_s}} < \left| \frac{2}{F} \right|_{z=e^{j\omega T_s}}, \omega \in [0, \pi/T_s] \tag{7}$$

Therefore, the closed-loop system is stable when the control gain satisfies the following condition.

$$0 < k_f < \left| \frac{2 + 2C_x G_{xx}}{F G_{xx}} \right|_{z=e^{j\omega T_s}} = \left| \frac{2}{F G_{xx}} + \frac{2C_x}{F} \right|_{z=e^{j\omega T_s}}, \omega \in [0, \pi/T_s] \tag{8}$$

It can be observed from Eq. (8) that the FIR low-pass filter should be able to effectively suppress the dominant lightly-damped resonant peak of the scanner to guarantee the availability of the stable control gain.

4. Experimental setup and controller implementation

4.1. Experimental setup

To demonstrate the effectiveness of the developed MFRC on AFM raster scanning, the experiments are conducted on a commercial AFM (NTMDT, Prima), which includes a piezoelectric tube scanner (PTS) for XYZ positioning. The experimental setup is shown in Fig. 4, which includes the PTS scanning module, the high-voltage amplifier (amplification ratio of 30) providing the actuation voltage for both lateral axes, the signal access module transferring the control signals to the PTS, and the integrated controller outputting the real time sensors signals, the rapid prototype control module (dSPACE, ds1103) running different control schemes and an auxiliary optical microscope adjusting the lasers and sample positions. Each axis of the PTS is equipped with a capacitive displacement sensor. The control schemes are designed with the environments of Matlab, downloaded to dSPACE host, and operated via the ControlDesk

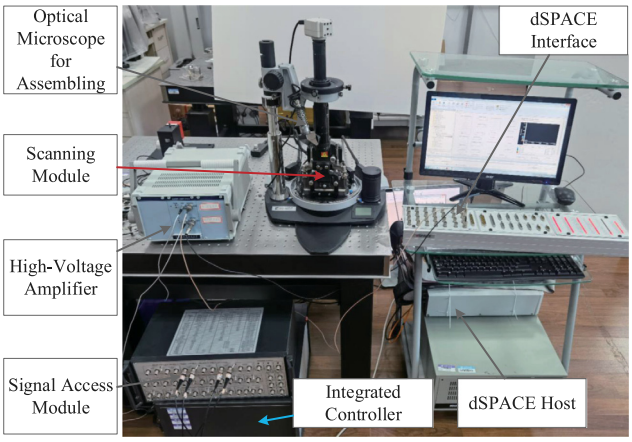

Fig. 4. Experimental setup verifying the advantages the developed MFRC scheme.

software. For generating the AFM images, a calibration grating (NTMDT, TGQ1) with a known rectangular profile (height of 20 nm, period of 3 μm) is placed on the scanner. The contact probe (Scansens, HA_C/15) with a resonance of 19 kHz and a force constant of 0.26 N/m is employed to measure the sample topography. The sampling frequency is 20 kHz and thus the imaging resolution is set as 100 × 100.

4.2. Controller implementation and performance evaluation

To show the complex dynamics of the scanner and the complicated cross-coupling effect, the dynamics of the lateral axes are investigated first. The low-amplitude band-limited noise signals are applied to excite the two axes respectively, and the actuation signals and the sensors signals are captured simultaneously. Via identification toolbox of Matlab, the obtained frequency responses are shown in Fig. 5. It can be observed from this figure that the cross-coupling effect shows complex dynamics, making it challenging for cross-coupling modeling. Meanwhile, the multi-modes can be found in the dynamics of the Y-axis. Another problem that usually exists in AFM applications is model uncertainties due to the load changes (including the sample and holders). To show this, the frequency responses with different samples (no load, with load L1 and with load L2) are analyzed and plotted in Fig. 5 as well. Taking the X-axis for example, its first-order resonant frequency varies from to 970 to 602 Hz, which is a quite large model uncertainty. This might lead to the instability of model-based control schemes. However, from Eq. (8), it can be concluded that it would be asymptotically stable for all cases when the closed-loop system is asymptotically stable for the extreme condition (Load L2 in this work). Without loss of generality, the two cases (with load L1 and L2) will be further studied.

Before the design of the developed MFRC, the baseline tracking controllers for the X- and Y-axis have to be optimized. To achieve sufficient tracking performance, the proportional and integral gains of the PI controller is maximized until the vibrations occur during step response using trial-and-error method, and the resulting parameters are 0.01 and 300 for the X-axis, and 0.01 and 250 for the Y-axis, respectively. These controller gains are used for all of the following experiments. Secondly, as the lowest resonant frequencies of the X-axis and Y-axis are about 602 Hz and 635 Hz, the stopband of $F(z)$ is set to 600 Hz. It is shown in Fig. 2 that tracking errors are mainly composed of the first three harmonics; therefore, the passband of $F(z)$ is set to 300 Hz. To guarantee the behavior of $F(z)$ within the passband, the Equiriple method [41] is employed to calculate the filter parameters. With the tradeoff of precision and causality of the developed MFRC, the order of $F(z)$ is chosen as 300. Based on the above parameters, the control gain k_f is optimized as 0.5 via experiments within the region of stability.

To further investigate the performance of the developed MFRC for tracking periodic trajectories and rejecting periodic disturbances, the magnitude responses of the repetitive loop $F(z)z^{-N+n_f}/(1-F(z)z^{-N+n_f})$ and the sensitivity functions (Eq. (3)) are presented for the X-axis in Fig. 6(a) and (b) (with Load L1 and Load L2) respectively for a tracking frequency of 100 Hz. It can be observed in Fig. 6(a) that the MFRC mainly generates control gain within the passband of 300 Hz, and thus rejects the tracking errors distributed within the passband. This can also be concluded from the sensitivity functions in Fig. 6(b). Additionally, it can also be seen in Fig. 6(b) that the sensitivity functions for the X-axis with different loads show similar disturbance rejection ability, demonstrating its robustness against model uncertainties.

5. Experimental studies

5.1. Tracking results of the X-axis

In raster scanning applications, the control objective for the X-axis is to track a pre-defined triangular trajectory, which is studied first in this section. The tracking experiments for the smoothed triangular trajectories and the triangular trajectories, with the

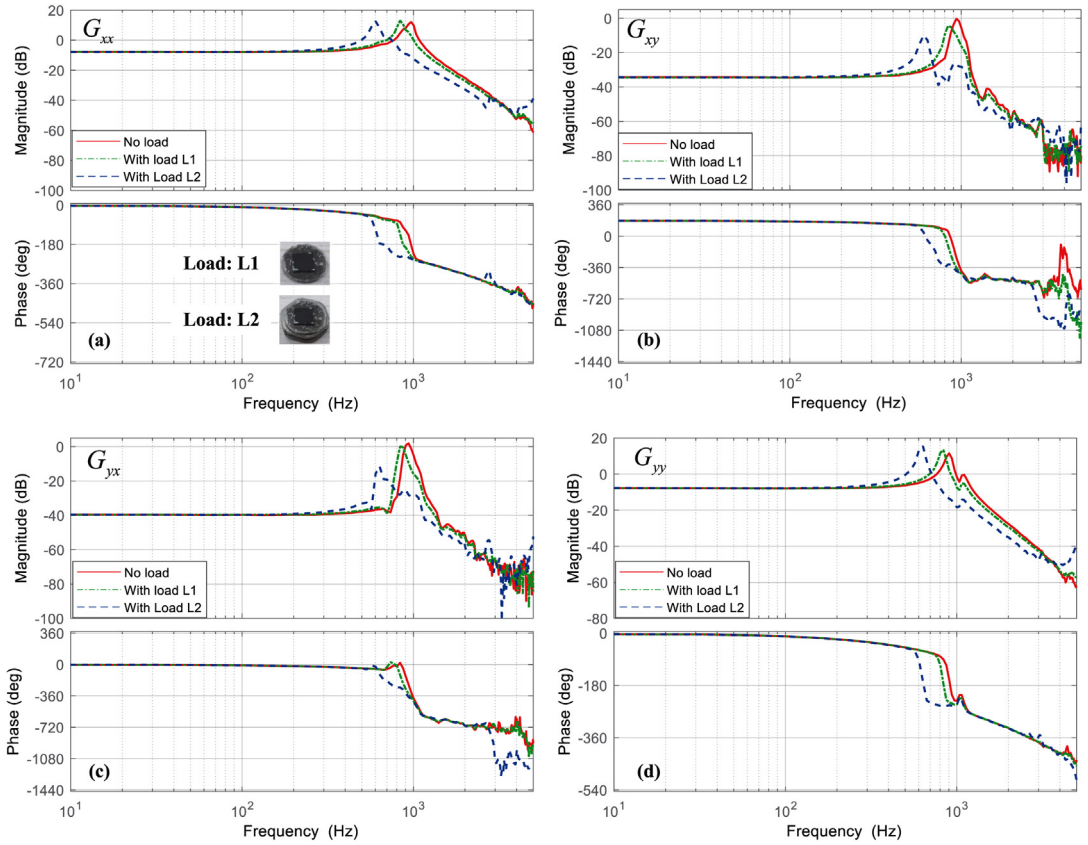

Fig. 5. Dynamics of the lateral axes of PTS with different loads: (a) X-axis; (b) The coupling effect from X-axis to Y-axis (G_{xy}); (c) The coupling effect from Y-axis to X-axis (G_{yx}); (d) Y-axis.

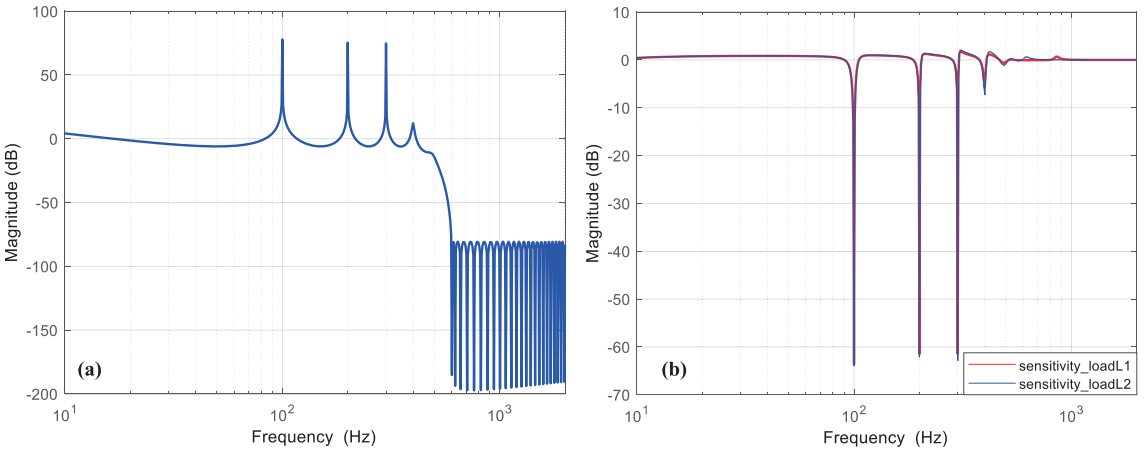

Fig. 6. Magnitude response of (a) $F(z)z^{-N+n_f}/(1-F(z)z^{-N+n_f})$ and (b) sensitivity functions, for a tracking frequency of 100 Hz.

scanning range of 10 μm × 10 μm and frequencies of 10, 50 and 100 Hz, are conducted using the developed PI+MFRC on the setup presented in Section 4. The tracking results of the scanner with the two different loads are presented in Fig. 7 for the frequency of 100 Hz as case studies. It can be found from Fig. 7 that similar convergence is achieved when tracking these two trajectories. Note that, to guarantee the same effective imaging trajectory with the traditional raster scanning, the amplitude of the designed smoothed trajectory is slightly larger than that of the triangular trajectory as illustrated in Fig. 7, but its high-frequency components are lower than those of the triangular trajectory, which would contribute to lower tracking errors. As shown in Fig. 7, the maximum

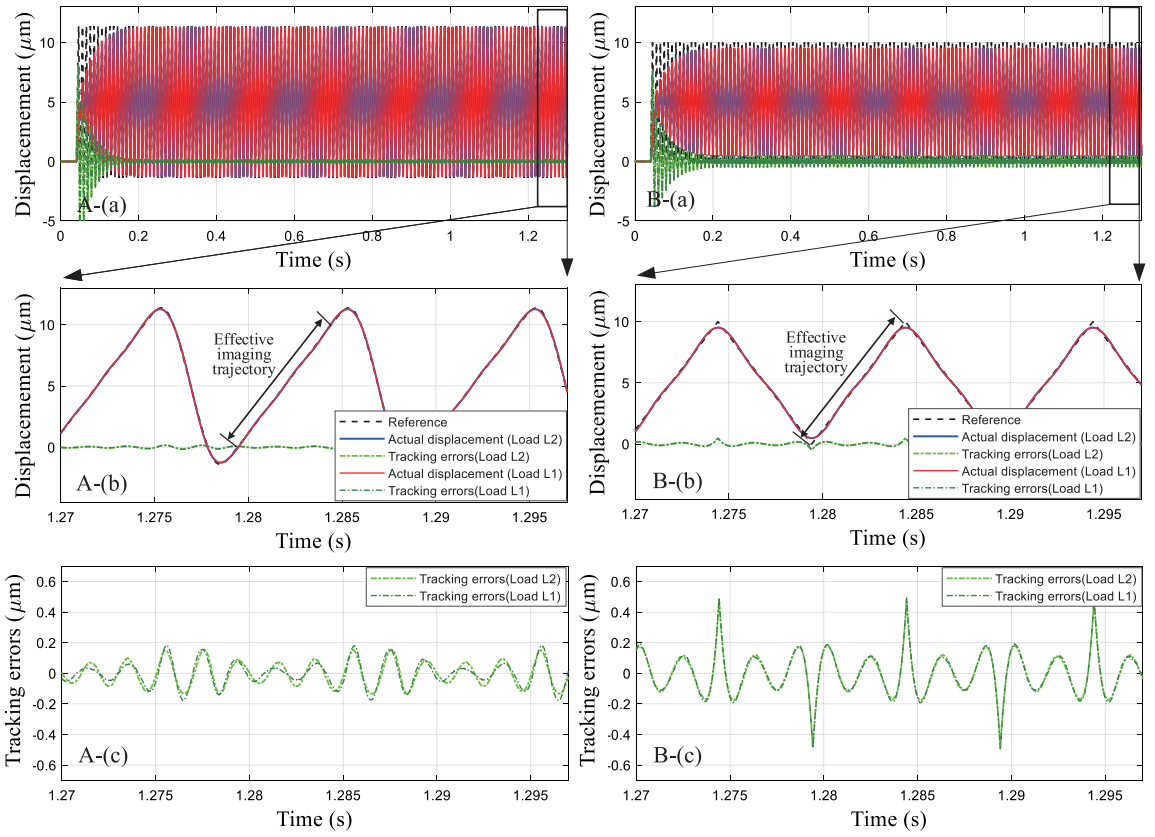

Fig. 7. Tracking results of the closed-loop system with different loads under the developed PI+MFRC for different trajectories with the frequency of 100 Hz: (A) smoothed trajectory; (B) triangular trajectory.

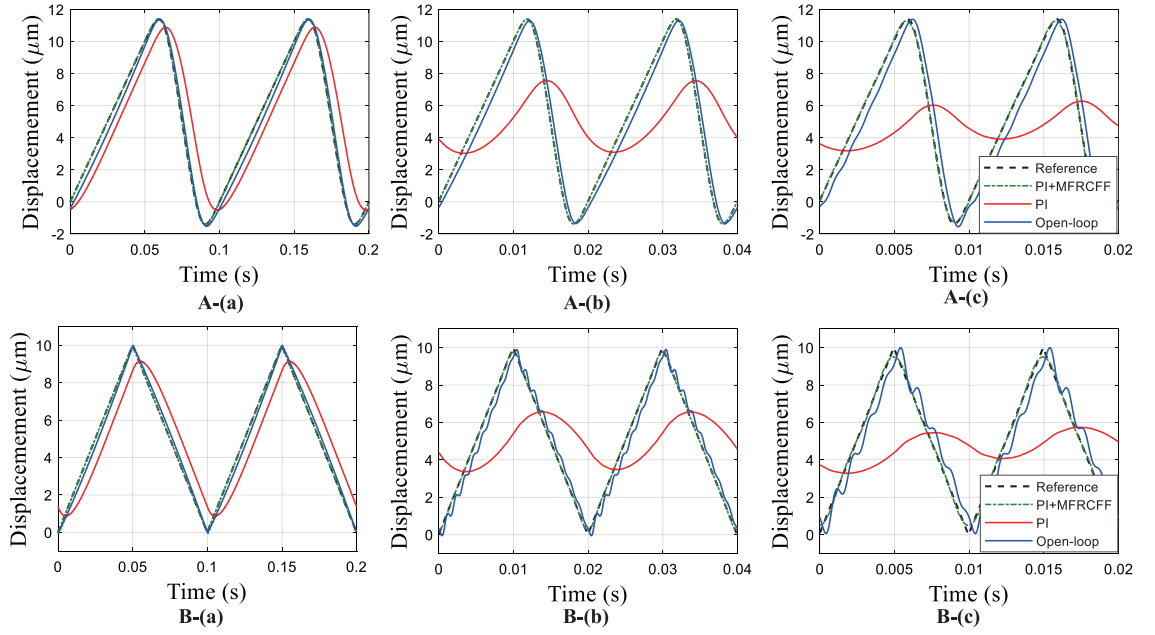

Fig. 8. Tracking results for the X-axis with different control schemes for different frequencies: (A) smoothed triangular trajectories; (B) triangular trajectories; (a) 10 Hz; (b) 50 Hz; (c) 100 Hz.

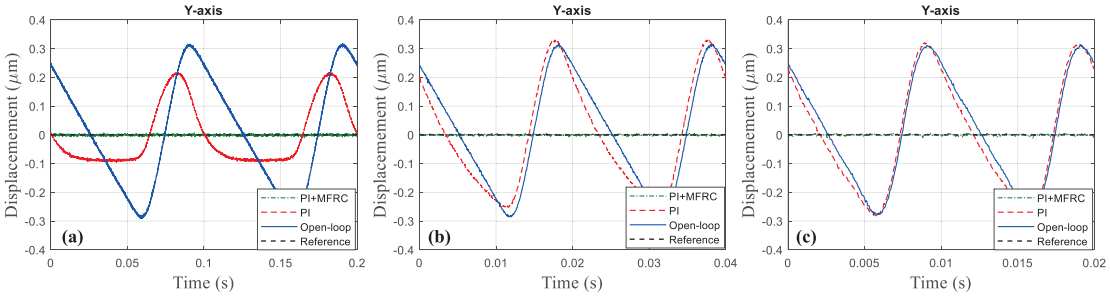

Fig. 9. The tracking results of the closed-loop system for Y-axis with different control schemes under different tracking frequencies: (a) 10 Hz; (b) 50 Hz; (c) 100 Hz.

Table 1
The coupling induced tracking errors in the Y-axis with different control schemes when X-axis is tracking smoothed triangular trajectories with the proposed PI+MFRCFF scheme under different frequencies.

Frequency	Open-loop (nm)		Baseline PI (nm)		PI+MFRC (nm)	
(Hz)	e_m	e_{rms}	e_m	e_{rms}	e_m	e_{rms}
10	317.9	191.4	218.7	107.1	7.6	2.5
50	315.3	191.0	330.6	188.5	7.6	2.6
100	312.8	191.4	320.4	194.6	7.6	2.8

tracking errors (with Load L1) for the effective imaging trajectory in the triangular trajectory is calculated as 0.4963 μm, which is reduced to 0.0839 μm for that in the smoothed triangular trajectory with improved harmonics components. From the convergence and the tracking errors in steady-state (Fig. 7(a) and (c)) for these two trajectories, it is observed that the tracking results of the scanner with different loads (L1 and L2) resemble each other, which verifies the robustness of the developed PI+MFRC against model uncertainties. Hence, the tracking results of the scanner with only load L1 are provided in subsequent section for illustrations.

Compared to other model-based repetitive control methods, the developed PI+MFRC scheme requires more iterations to converge to steady-state. To address this issue, the corresponding control signals $u_{ffx}(k)$ (in Fig. 3) are captured and recorded. These control signals are then regarded as the offline-learned MFRC based feedforward control (MFRCFF), which is combined with the baseline PI controller forming the proposed PI+MFRCFF scheme. In this case, the MFRC in Fig. 3(a) is substituted by $u_{ffx}(k)$. The tracking results of the smoothed triangular trajectories with frequencies of 10, 50, and 100 Hz are shown in Fig. 8 (A), where high performance tracking control is achieved in terms of the tracking precision and convergence speed. To show its advantages, the comparative experiments are conducted with different control schemes, which are the baseline PI control and open-loop control. The tracking results of X-axis for triangular trajectories with different tracking frequencies are also plotted in Fig. 8 (B). In this figure, it is seen that the hysteresis nonlinearity and vibration cause large tracking errors in open-loop, which are both mitigated by the proposed PI+MFRCFF scheme. The tracking performance of the baseline PI controller is also significantly improved greatly by adding the MFRCFF scheme. These results verify the advantages of the proposed PI+MFRCFF scheme in tracking periodic trajectories. As the smoothed raster scanning and tradition raster scanning share the same effective imaging trajectory (the forward path in this work), the smoothed raster scanning [37] is employed in this work for high-precision scanning applications in subsequent sections.

5.2. Tracking results of the Y-axis

To investigate the coupling effect from the X-axis to the Y-axis, the tracking results of Y-axis for a constant setpoint (zero) and different control schemes are presented in Fig. 9. In these results, the X-axis is tracking a smoothed triangular trajectory using the proposed PI+MFRCFF scheme with a tracking frequency of 10, 50 and 100 Hz. As shown in Fig. 5(b), the coupling dynamics from the X-axis to Y-axis is approximately constant within the frequencies below 300 Hz, so the coupled tracking errors of the Y-axis in open-loop show similar profiles for all tested frequencies. When the Y-axis is under PI control, the coupled tracking errors increase with frequency due to the narrow control bandwidth. For frequencies of 50 Hz and 100 Hz, the error under PI control is similar with those in open-loop, which will cause failure of coupling compensation. In contrast, the tracking results of the Y-axis with the developed PI+MFRC show excellent coupling error rejection.

To evaluate the coupling compensation performance, two metrics are calculated, which are the maximum tracking error

$$e_m = \max_{t\in(0,2T]} \left|y_d(t) - y_a(t)\right| \tag{9}$$

and the root-mean-square (RMS) tracking error

$$e_{rms} = \sqrt{\frac{1}{2T}\int_0^{2T} [y_d(t) - y_a(t)]^2 dt} \tag{10}$$

The results are summarized in Table 1. It can be seen that, for all the tested frequencies, the coupled tracking errors obtained with the PI+MFRC are reduced greatly as compared with those obtained with the open-loop control and with the baseline PI control.

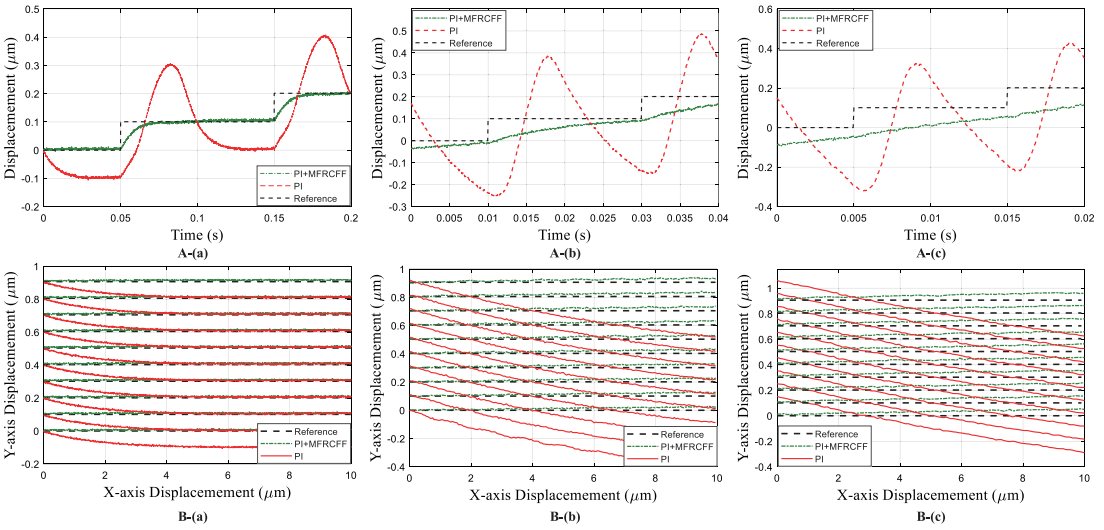

Fig. 10. Tracking results of the closed-loop system (with X-axis under PI+MFRCFF and Y-axis under different control schemes) for different scanning rates: (a) 10-Hz; (b) 50-Hz; (c) 100-Hz; (A) tracking results of Y-axis; (B) tracking results in X–Y plane.

Specifically, the RMS of the coupled tracking errors under the PI+MFRC is reduced from 191.0 nm (under the open-loop control) and 188.5 nm (under the baseline PI control) to 2.6 nm at the frequency of 50 Hz, which are reduced by 98.48% and 98.62% respectively. And for the frequency of 100 Hz, it is reduced from 191.4 nm (under the open-loop control) and 194.6 nm (under baseline PI control) to 2.8 nm, which are reduced by 98.54% and 98.56% respectively. Therefore, it is demonstrated that the developed PI+MFRC scheme is effective for coupling compensation as well.

5.3. Raster scanning and imaging results

In scanning applications, the Y-axis follows non-periodic staircase trajectory, which hinders the application the developed PI+MFRC scheme. To deal with this problem, the proposed MFRCFF in Section 5.1 is employed herewith, in which the MFRC learned control signals $u_{ffy}(k)$ are used as the feedforward controller. In this case, the MFRC in Fig. 3(b) is substituted by the $u_{ffy}(k)$. To study the effectiveness of the proposed PI+MFRCFF, the smoothed raster scanning experiments are conducted. The tracking results of the X-axis for smoothed triangular trajectories are shown in Fig. 8(A), while the tracking results of the Y-axis for staircase trajectories and the corresponding raster scanning results (10 lines) are presented in Fig. 10 for the scanning rates of 10-, 50-, and 100-Hz. It can be observed in detail that the scanning trajectories tilt from the desired positions with PI control due to the coupling effect, especially for the scanning rates of 50- and 100-Hz. Since the coupled errors are well compensated using the proposed PI+MFRCFF scheme, raster scanning with this approach generates excellent tracking. Note that due to the narrow bandwidth of the baseline PI control, the tracking performance of the staircase trajectories (under the proposed PI+MFRCFF control) degrades with increasing scanning rate, which can be improved by other high-bandwidth tracking methods.

To illustrate the effectiveness of the proposed PI+MFRCFF scheme on AFM imaging applications (especially on coupling compensation), the calibration grating is imaged in Fig. 11. The AFM is operated in constant height mode, which implies that the deflection signals of the cantilever are used for generating the AFM images. In Fig. 11, the results obtained with PI control are illustrated in the first row and the results obtained with the proposed PI+ MFRCFF scheme are illustrated in the second row. Since all images are captured using the proposed PI+MFRCFF scheme for X-axis, the imaging results show the same features along the X-axis. However, it can be clearly observed in Fig. 11 that the captured topography under PI control is severely rotated due to the coupling errors along the Y-axis. This problem is well addressed using the proposed PI+MFRCFF scheme.

6. Conclusion

In this article, a model-free repetitive control (MFRC) is proposed to address the difficulties associated with plant inversion for tracking periodic trajectories and rejecting periodic disturbances. Its effectiveness is evaluated in AFM raster scanning, whose objective is to achieve fast reference tracking in the X-axis while compensating for the coupling effect on the Y-axis. By employing a non-causal FIR low-pass filter to replace the normally used two-step design method (low-pass filter and plant inversion, required by the model-based repetitive control design), the proposed method avoids the need for an inverse system model, which makes it rather simple for practical implementations. Stability analysis is presented to provide criteria for determining controller parameters. The efficacy of the developed MFRC scheme is successfully evaluated by controlling an AFM scanner under varying load conditions. The tracking results of X-axis show the excellent robustness against the model uncertainties, but slower convergence. With the improved

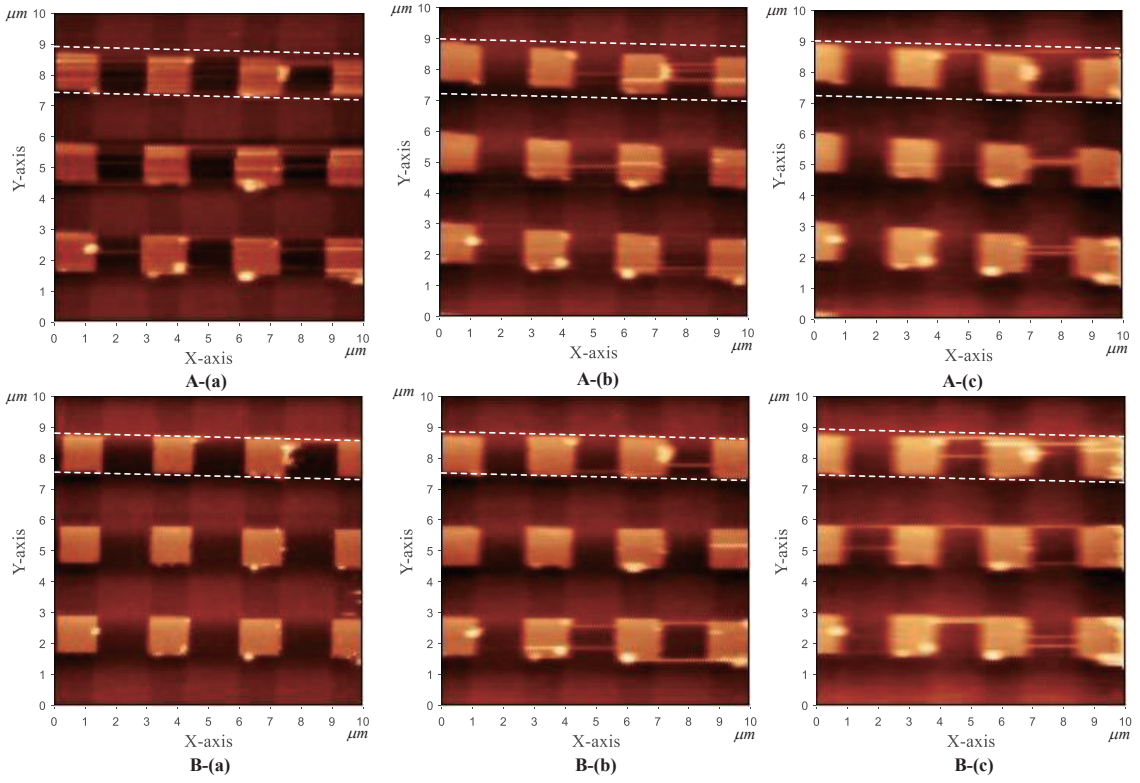

Fig. 11. AFM imaging results using smoothed raster scanning for different scanning rates and Y-axis with (A) PI and (B) PI+MFRCFF; for the scanning rate of (a) 10-Hz; (b) 50-Hz; (c) 100-Hz.

harmonic components, the smoothed raster scanning is finally utilized to generate the scanning trajectories as well as capture the AFM images. To achieve fast convergence in the X-axis and coupling compensation while tracking staircase trajectories in the Y-axis, a pre-learning step is utilized to generate the corresponding control signals, which are combined with the baseline PI controller in a feedforward manner. Experimental results on a piezoelectric tube scanner show significant reductions in X-axis tracking error and Y-axis coupling errors, and high performance raster scanning is achieved for a scanning rate of 100-Hz.

Declaration of competing interest

The authors declare that they have no known competing financial interests or personal relationships that could have appeared to influence the work reported in this paper.

Acknowledgments

This work was partially supported by the National Natural Science Foundation of China (Grant Nos. 52105581, U2013211, and 51975375), the China Postdoctoral Science Foundation (No. 2021M692065), the Open Foundation of the State Key Laboratory of Fluid Power and Mechatronic Systems, China (Grant No. GZKF-202003), and the CDSC Scholarship, University of Newcastle, Australia, awarded to Linlin Li.

References

[1] G. Binnig, C.F. Quate, C. Gerber, Atomic force microscope, Phys. Rev. Lett. 56 (1896) 930–933.
[2] M. Krieg, G. Flaschner, D. Alsteens, et al., Atomic force microscopy-based mechanobiology, Nat. Rev. Phys. 1 (2019) 41–57, http://dx.doi.org/10.1038/s42254-018-0001-7.
[3] X. Chen, J. Lai, Y. Shen, Q. Chen, L. Chen, Functional scanning force microscopy for energy nanodevices, Adv. Mater. 30 (48) (2018) 1802490, http://dx.doi.org/10.1002/adma.201802490.
[4] M.S. Rana, H.R. Pota, I.R. Petersen, Improvement in the imaging performance of atomic force microscopy: A survey, IEEE Trans. Autom. Sci. Eng. 14 (2) (2017) 1265–1285, http://dx.doi.org/10.1109/TASE.2016.2538319.
[5] S.K. Das, F.R. Badal, Md. A. Rahman, et al., Improvement of alternative non-raster scanning methods for high speed atomic force microscopy: A review, IEEE Access 7 (2019) 115603-115624, http://dx.doi.org/10.1109/ACCESS.2019.2936471.

[6] L. Li, C.-X. Li, G. Gu, L. Zhu, Modified repetitive control based cross-coupling compensation approach for the piezoelectric tube scanner of atomic force microscopes, IEEE/ASME Trans. Mechatron. 24 (2) (2019) 666–676, http://dx.doi.org/10.1109/TMECH.2019.2893628.

[7] Y. Wu, Q. Zou, Iterative control approach to compensate for both the hysteresis and the dynamics effects of piezo actuators, IEEE Trans. Control Syst. Technol. 15 (5) (2007) 936–944, http://dx.doi.org/10.1109/TCST.2007.899722.

[8] C.-X. Li, G.-Y. Gu, M.-J. Yang, L.-M. Zhu, High-speed tracking of a nanopositioning stage using modified repetitive control, IEEE Trans. Autom. Sci. Eng. 14 (3) (2017) 1467–1477, http://dx.doi.org/10.1109/TASE.2015.2428437.

[9] Q. Xu, Adaptive integral terminal third-order finite-time sliding-mode strategy for robust nanopositioning control, IEEE Trans. Ind. Electron. 68 (7) (2021) 6161–6170, http://dx.doi.org/10.1109/TIE.2020.2998751.

[10] L. Kong, D. Li, J. Zou, W. He, Neural networks based learning control for a piezoelectric nanopositioning system, IEEE/ASME Trans. Mechatron. 25 (6) (2020) 2904–2914, http://dx.doi.org/10.1109/TMECH.2020.2997801.

[11] G.-Y. Gu, L.-M. Zhu, C.-Y. Su, H. Ding, S. Fatikow, Modeling and control of piezo-actuated nanopositioning stages: A survey, IEEE Trans. Autom. Sci. Eng. 13 (1) (2016) 313–332, http://dx.doi.org/10.1109/TASE.2014.2352364.

[12] V. Hassani, T. Tjahjowidodo, T.N. Do, A survey on hysteresis modeling, identification and control, Mech. Syst. Signal Process. 49 (1–2) (2014) 209–233, http://dx.doi.org/10.1016/j.ymssp.2014.04.012.

[13] D.V. Sabarianand, P. Karthikeyan, T. Muthuramalingam, A review on control strategies for compensation of hysteresis and creep on piezoelectric actuators based micro systems, Mech. Syst. Signal Process. 140 (2020) 106634, http://dx.doi.org/10.1016/j.ymssp.2020.106634.

[14] P.-K. Wong, Q. Xu, C.-M. Vong, H.-C. Wong, Rate-dependent hysteresis modeling and control of a piezostage using online support vector machine and relevance vector machine, IEEE Trans. Ind. Electron. 59 (4) (2012) 1988–2001, http://dx.doi.org/10.1109/TIE.2011.2166235.

[15] K. Cai, X. He, Y. Tian, et al., Design of a XYZ scanner for home-made high-speed atomic force microscopy, Microsyst. Technol. 24 (7) (2018) 3123–3132, http://dx.doi.org/10.1007/s00542-017-3674-4.

[16] D.S. Raghunvanshi, S.I. Moore, A.J. Fleming, Y.K. Yong, Electrode configurations for piezoelectric tube actuators with improved scan range and reduced cross-coupling, IEEE/ASME Trans. Mechatron. 25 (3) (2020) 1479–1486, http://dx.doi.org/10.1109/TMECH.2020.2978241.

[17] C.-X. Li, G.-Y. Gu, M.-J. Yang, L.-M. Zhu, Design, analysis and testing of a parallel-kinematic high-bandwidth XY nanopositioning stage, Rev. Sci. Instrum. 84 (12) (2013) 125111, http://dx.doi.org/10.1063/1.4848876.

[18] K.K. Leang, S. Devasia, Feedback-linearized inverse feedforward for creep, hysteresis, and vibration compensation in AFM piezoactuators, IEEE Trans. Control Syst. Technol. 15 (5) (2007) 927–935.

[19] A.J. Fleming, A.G. Wills, Optimal periodic trajectories for band-limited systems, IEEE Trans. Control Syst. Technol. 17 (3) (2009) 552–562, http://dx.doi.org/10.1109/TCST.2008.2001375.

[20] B. Bhikkaji, M. Ratnam, S.O.R. Moheimani, PVPF control of piezoelectric tube scanners, Sens. Actuators Phys. 135 (2) (2007) 700–712, http://dx.doi.org/10.1016/j.sna.2006.07.032.

[21] L. Li, C.-X. Li, G. Gu, L.-M. Zhu, Positive acceleration, velocity and position feedback based damping control approach for piezo-actuated nanopositioning stages, Mechatronics 47 (2017) 97–104, http://dx.doi.org/10.1016/j.mechatronics.2017.09.003.

[22] M. Namavar, A.J. Fleming, M. Aleyaasin, et al., An analytical approach to integral resonant control of second-order systems, IEEE/ASME Trans. Mechatron. 19 (2) (2014) 651–659, http://dx.doi.org/10.1109/TMECH.2013.2253115.

[23] M.-J. Yang, J.-B. Niu, C.-X. Li, et al., High-bandwidth control of nanopositioning stages via an inner-loop delayed position feedback, IEEE Trans. Autom. Sci. Eng. 12 (4) (2015) 1357–1368, http://dx.doi.org/10.1109/TASE.2015.2451368.

[24] G.M. Clayton, S. Tien, K.K. Leang, Q. Zou, S. Devasia, A review of feedforward control approaches in nanopositioning for high-speed SPM, J. Dyn. Syst. Meas. Control 131 (6) (2009) 061101, http://dx.doi.org/10.1115/1.4000158.

[25] Y.K. Yong, S.O.R. Moheimani, B.J. Kenton, K.K. Leang, Invited review article: High-speed flexure-guided nanopositioning: Mechanical design and control issues, Rev. Sci. Instrum. 83 (12) (2012) 121101, http://dx.doi.org/10.1063/1.4765048.

[26] Y. Shan, K.K. Leang, Accounting for hysteresis in repetitive control design: Nanopositioning example, Automatica 48 (8) (2012) 1751–1758, http://dx.doi.org/10.1016/j.automatica.2012.05.055.

[27] L. Li, Z. Chen, S.S. Aphale, L.M. Zhu, Fractional repetitive control of nanopositioning stages for high-speed scanning using low-pass FIR variable fractional delay filter, IEEE/ASME Trans. Mechatron. 25 (2) (2020) 547–557, http://dx.doi.org/10.1109/TMECH.2020.2969222.

[28] Z. Feng, M. Ming, J. Ling, et al., Fractional delay filter based repetitive control for precision tracking: Design and application to a piezoelectric nanopositioning stage, Mech. Syst. Signal Process. 164 (2022) 108249, http://dx.doi.org/10.1016/j.ymssp.2021.108249.

[29] H. Xie, Y. Wen, X. Shen, H. Zhang, L. Sun, High-speed AFM imaging of nanopositioning stages using H_∞ and iterative learning control, IEEE Trans. Ind. Electron. 67 (3) (2020) 2430–2439, http://dx.doi.org/10.1109/TIE.2019.2902792.

[30] Z. Li, J. Shan, Modeling and inverse compensation for coupled hysteresis in piezo-actuated Fabry–Perot spectrometer, IEEE/ASME Trans. Mechatron. 22 (4) (2017) 1903–1913, http://dx.doi.org/10.1109/TMECH.2017.2703167.

[31] M.S. Rana, H.R. Pota, I.R. Petersen, Nonlinearity effects reduction of an AFM piezoelectric tube scanner using MIMO MPC, IEEE/ASME Trans. Mechatron. 20 (3) (2015) 1458–1469, http://dx.doi.org/10.1109/TMECH.2014.2356454.

[32] M.S. Rana, H.R. Pota, I.R. Petersen, Spiral scanning with improved control for faster imaging of AFM, IEEE Trans. Nanotechnol. 13 (3) (2014) 541–550, http://dx.doi.org/10.1109/TNANO.2014.2309653.

[33] Y.K. Yong, K. Liu, S.O.R. Moheimani, Reducing cross-coupling in a compliant XY nanopositioner for fast and accurate raster scanning, IEEE Trans. Control Syst. Technol. 18 (5) (2010) 1172–1179, http://dx.doi.org/10.1109/TCST.2009.2033201.

[34] H. Habibullah, H.R. Pota, I.R. Petersen, M.S. Rana, Creep, hysteresis, and cross-coupling reduction in the high-precision positioning of the piezoelectric scanner stage of an atomic force microscope, IEEE Trans. Nanotechnol. 12 (6) (2013) 1125–1134, http://dx.doi.org/10.1109/TNANO.2013.2280793.

[35] S.I. Moore, Y.K. Yong, M. Omidbeike, A.J. Fleming, Serial-kinematic monolithic nanopositioner with in-plane bender actuators, Mechatronics 75 (2021) 102541, http://dx.doi.org/10.1016/j.mechatronics.2021.102541.

[36] S.K. Das, H.R. Pota, I.R. Petersen, Damping controller design for nanopositioners: A mixed passivity, negative-imaginary, and small-gain approach, IEEE/ASME Trans. Mechatron. 20 (1) (2015) 416–426, http://dx.doi.org/10.1109/TMECH.2014.2331321.

[37] L. Li, J. Huang, S.S. Aphale, L.M. Zhu, A smoothed raster scanning trajectory based on acceleration-continuous B-spline transition for high-speed atomic force microscopy, IEEE/ASME Trans. Mechatron. 26 (1) (2021) 24–32, http://dx.doi.org/10.1109/TMECH.2020.2995156.

[38] S. Tien, Q. Zou, S. Devasia, Iterative control of dynamics-coupling-caused errors in piezoscanners during high-speed AFM operation, IEEE Trans. Control Syst. Technol. 13 (6) (2005) 921–931, http://dx.doi.org/10.1109/TCST.2005.854334.

[39] Y. Tian, K. Cai, D. Zhang, et al., Development of a XYZ scanner for home-made atomic force microscope based on FPAA control, Mech. Syst. Signal Process. 131 (2019) 222–242, http://dx.doi.org/10.1016/j.ymssp.2019.05.057.

[40] Z. Feng, W. Liang, J. Ling, et al., Integral terminal sliding-mode-based adaptive integral backstepping control for precision motion of a piezoelectric ultrasonic motor, Mech. Syst. Signal Process. 144 (2020) 106856, http://dx.doi.org/10.1016/j.ymssp.2020.106856.

[41] A.V. Oppenheim, R.W. Schafer, J.R. Buck, Discrete-Time Signal Processing, second ed., Prentice-Hall, Inc., 1999.